This is to certify that the
thesis entitled

AN INVESTIGATION OF MODEL REFERENCE ADAPTIVE CONTROL OF UNKNOWN DYNAMIC HYSTERETIC SYSTEMS USING SLOW ADAPTATION

presented by

James J Reynolds

has been accepted towards fulfillment
of the requirements for the

Master of Science degree in Electrical and Computer Engineering

Hassan Khalil
Major Professor's Signature

December 7, 2007
Date

AN INVESTIGATION OF MODEL REFERENCE ADAPTIVE CONTROL OF UNKNOWN DYNAMIC HYSTERETIC SYSTEMS USING SLOW ADAPTATION

By

James J Reynolds

A THESIS

Submitted to
Michigan State University
in partial fulfillment of the requirements
for the degree of

MASTER OF SCIENCE

Department of Electrical and Computer Engineering

2007

ABSTRACT

AN INVESTIGATION OF MODEL REFERENCE ADAPTIVE CONTROL OF UNKNOWN DYNAMIC HYSTERETIC SYSTEMS USING SLOW ADAPTATION

By

James J Reynolds

This thesis is a first step in analyzing model reference adaptive control of an unknown linear system preceded by an unknown hysteresis nonlinearity. The parameters of the hysteresis nonlinearity are adapted much slower than the parameters of the linear system, which are in turn adapted much slower than the plant dynamics. This approach allows the system to be considered under an averaging framework, where slower variables are viewed as constant with respect to faster variables. The problem statement is established and the first steps in analyzing the system are laid out. Challenges that arise in this problem beyond a classical averaging or singular perturbation problem are outlined. Simulation is used to not only show the effectiveness of the control method, but also to gain some additional insight into properties and behaviors of the closed-loop system.

For my Mother, Earaina Lynn, and my biggest supporter, Jennifer Lynn.

ACKNOWLEDGEMENTS

I would like to express my sincerest thanks to those who made this work possible. Without their guidance, support and unwavering patience, I could never have known where or how to begin this project, or how far I could stretch my own abilities. I would like to specifically thank Dr. Hassan Khalil and Dr. Xiaobo Tan for all of their time, effort and invaluable advice. I would also like to thank Dr. Ning Xi for serving on the committee for this thesis.

TABLE OF CONTENTS

LIST OF TABLES

LIST OF FIGURES

1. Introduction

Model reference adaptive control (MRAC) of systems with hysteresis nonlinearities has recently become a topic of interest, in particular regarding control of smart materials [1, 2, 3]. A hysteresis operator preceding linear dynamics will be used to model these systems. Refer to Fig. 1.1.

There are many different hysteresis models. In [4, 5], Tao and Kokotovic consider a piecewise linear hysteresis model. This model has a small number of parameters that describe it. It will lead to computational simplicity at the expense of model accuracy. Overparameterization by way of a Kronecker product is used to accommodate the bilinear coupling of parameters. Because of the inaccuracy in this model, Tan and Khalil instead used a Preisach hysteresis model [6]. The same bilinear coupling of parameters is present with a Preisach model as the piecewise linear model. For n_H and n_P parameters associated with the hysteresis operator and linear dynamics, respectively, overparameterization will give $n_H n_P$ parameters. The number of parameters of a Preisach operator can be quite large, meaning the use of overparameterization will require a cumbersome amount of computation. For example, in [7], Tan and Baras used a 10-level discretization of the Preisach plane which results in 56 hysteresis parameters. For a linear plant with denominator of degree three, overparameterization will give 112 parameters from the Kronecker product. To alleviate this difficulty, Tan and Khalil instead proposed using slow adaptation to create a separation of time scales. In this way, the number of parameters remains manageable; 58 parameters in the above example. Slow adaptation also allows the behavior of the plant parameter adaptation and hysteresis parameter adaptation, as well as the closed-loop stability,

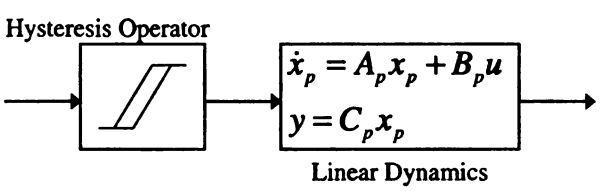

Figure 1.1: A hysteresis operator preceding linear dynamics.

to be evaluated using averaging and singular perturbation techniques.

For both hysteresis models (piecewise linear and Preisach) the output is shown to be the inner product of a regressor vector and a vector of available signals (and possibly an additive error term that results from inaccuracy in modelling). For this reason, the analysis of an MRAC with slowly adapted parameters should apply to either model (and any other hysteresis model whose output has the same structure), though slow adaptation will only be beneficial when the number of hysteresis parameters is large. The focus of this thesis will not be on the choice of a hysteresis model, but the performance and robustness of an MRAC with slow adaptation when the hysteresis model satisfies certain assumptions.

There are two major goals in this thesis: to begin the analysis of an MRAC with slowly adapted parameters with current averaging techniques and identify the obstacles in completing the analysis, and to perform simulations that will provide useful insight into the behavior of the complete nonlinear system. The majority of the analysis herein will rely heavily on "linearization" of the closed-loop system, and will only provide local information regarding its behavior. Therefore, simulations will be used as motivation for continuing this work and observing the stability requirements, convergence rates, basins of attraction, etc.

The thesis is structured as follows. Sections 2.1 and 2.2 derive the Preisach operator and introduce useful relationships between the operator and its inverse. Section 3.1 formulates the closed-loop system equations, using a similar method to that of Sastry and Bodson [8]. The uniqueness of the solution is established in Section 3.2. The parameter adaptation rules are derived in Section 3.3, using a simple gradient law. Section 4.1 reiterates an identification problem from [6] to motivate Section 4.2, where the closed-loop system is analyzed. This is the first known work establishing the closed-loop stability of MRAC systems with inverse hysteresis compensation and slow parameter adaptation. The theorems for stability rely on "linearization" of the closed-loop system about the origin, averaging techniques in [8] and singular perturbation techniques from [9]. Linearization is

used loosely here, because the system is not described by a pure *ordinary differential equation* (ODE). Section 4.3 provided local Lyapunov analysis based on a converse Lyapunov function argument. The Lyapunov stability of the system implies that the approximations from Section 3.3 are appropriate. Sections 5.1 and 5.2 give simulation results illustrating stability and parameter convergence and insight on the region of attraction, respectively. Future work and research goals are highlighted in Section 6.

2. Hysteresis Operator Review

The particular hysteresis operator used in this thesis, both for theoretical and simulation purposes is the *Preisach* operator. For a more detailed discussion of the Preisach operator one can refer to [10]. In [7] Tan and Baras show that with sufficiently large numbers of parameters a Preisach operator accurately describes the hysteresis in a magnetorestrictive actuator, and that continually increasing the number of parameters has limited benefits. This indicates that for a particular actuator, the dimensionality of the problem can be changed to optimize the performance, with a tradeoff between computational complexity and model accuracy. Because of this versatility of the Preisach operator it is preferable to a piecewise continuous operator as in [4, 5], which can only accurately describe very simple hysteretic phenomena.

The method for inverting the Preisach operator used in simulations in this thesis is described in [3]. The algorithm therein results in the exact inverse of a given Preisach operator after several iterations. The iterative nature of the inversion method requires a discrete-time implementation, with system sampling period greater than the necessary inversion time.

2.1 *The Preisach Operator*

The basic building block of a Preisach operator is a hysteron. A hysteron is a delayed relay, $\varphi_{\beta,\alpha}[\cdot,\cdot]$, with output either $+1$ or -1, where $\alpha \geq \beta$ are the switching thresholds. Fig. 2.1 shows the input-output curve of a generic hysteron. The arrows on the figure show the direction of the delay behavior. For $v \in C([0,T])$ and an initial configuration $\varphi_0 \in \{-1,1\}$, $\omega = \varphi_{\beta,\alpha}[v,\varphi_0]$ is defined as

$$\omega(t) \triangleq \begin{cases} +1 & \alpha < v(t), \\ -1 & \beta > v(t), \\ \omega(t^-) & \text{otherwise}, \end{cases} \qquad \text{for } t \in [0,T] \tag{2.1}$$

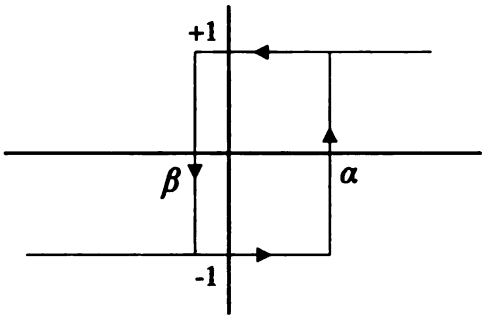

Figure 2.1: Input-output relationship of a hysteron operator.

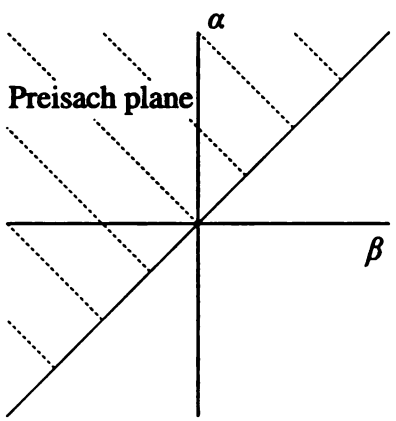

Figure 2.2: The Preisach plane.

where $\omega(0^-) \stackrel{\triangle}{=} \varphi_0$ and

$$t^- \stackrel{\triangle}{=} \lim_{\varepsilon>0, \varepsilon \to 0} t - \varepsilon,$$

as in [3]. From (2.1) it is clear that the current output of the hysteron operator depends on the output history. The hysteron operator has *memory*, as is typical of natural hysteretic phenomena. Define the *Preisach plane* as

$$\mathscr{P} \stackrel{\triangle}{=} \{(\beta, \alpha) \in \mathbb{R}^2 : \beta \leq \alpha\}. \tag{2.2}$$

The Preisach plane is clearly one half of $\mathbb{R}^2$, as shown in Fig. 2.2. In addition to the

Preisach plane, define the weighting function

$$\mu(\beta,\alpha) \geq 0 \,\forall (\beta,\alpha) \in \mathscr{P}. \tag{2.3}$$

The weighting function scales the portion of the Preisach operator output associated with a (β,α) pair. The Preisach operator, Γ, has output

$$u(t) = \int_{\mathscr{P}} \mu(\beta,\alpha)\varphi_{\beta,\alpha}[v,\varphi_0(\beta,\alpha)](t)d\beta d\alpha. \tag{2.4}$$

In the most general case, the Preisach operator depends on an infinite collection of hysterons and their respective weights, making it infeasible to implement. Therefore, a truncated region of the Preisach plane will be used and divided into K cells. The *discretization level*, L, is the number of cells in either the α or β direction. This means the number of resulting cells is $K = L(L+1)/2$. Define the truncated Preisach plane as

$$\mathscr{P}_T \triangleq \left\{(\beta,\alpha) \in \mathbb{R}^2 : \beta \leq \alpha \text{ and } \beta_{\min} \leq \beta \text{ and } \alpha \leq \alpha_{\max}\right\}.$$

Truncating the Preisach plane will limit the minimum and maximum output levels of the Preisach operator, which is acceptable as many real actuators will have a limited range of motion. Fig. 2.3 shows an example of a truncated Preisach plane with $L = 4$ and $K = 10$. Within each cell of the truncated Preisach plane, the weighting function is assumed to be uniform, i.e.

$$\mu(\beta,\alpha) = \theta_{H,k} \,\forall\, (\beta,\alpha) \in k^{th} \text{ cell}. \tag{2.5}$$

The *signed area* of the k^{th} cell, $w_{H,k}$, is defined as the *lower area*, C_k^+, minus the *upper area*, C_k^-. These areas are defined as

$$C_k^{\pm} = \left\{(\beta,\alpha) \in k^{th} \text{ cell} : \varphi_{\beta,\alpha}[v,\varphi_0](t) = \pm 1\right\}. \tag{2.6}$$

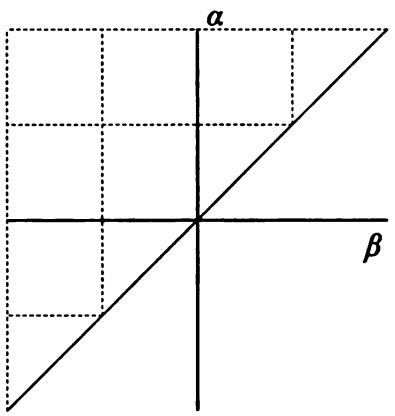

Figure 2.3: The discretized Preisach plane, with discretization level $L = 4$.

The total area of any cell is unity, i.e. if $\varphi_{\beta,\alpha}[v, \varphi_0](t) = +1\ (-1)\ \forall\ (\beta, \alpha) \in k^{th}$ cell, then $w_{H,k}(t) = +1\ (-1)$. The output of the truncated Preisach operator can now be written as

$$u(t) = \sum_{k=1}^{K} w_{H,k}\theta_{H,k} + \theta_{H,0}, \tag{2.7}$$

where $\theta_{H,0}$ is the contribution from hysterons outside of the discretized Preisach plane. If the truncated Preisach plane underestimates the range of the actuator, there will be a set of hysterons that can never change states. From this point on, (2.7) will be expressed as the inner product

$$u(t) = \theta_H^T w_H(t), \tag{2.8}$$

where

$$w_H(t) = \begin{bmatrix} 1 \\ w_{H,1}(t) \\ \vdots \\ w_{H,K}(t) \end{bmatrix}, \quad \theta_H = \begin{bmatrix} \theta_{H,0} \\ \theta_{H,1} \\ \vdots \\ \theta_{H,K} \end{bmatrix}. \tag{2.9}$$

Schematically, from this point on, the Preisach operator will be represented as a block labeled Γ as in Fig. 2.4.

The regressor in (2.9) is known for all time t, provided the initial *memory curve* is

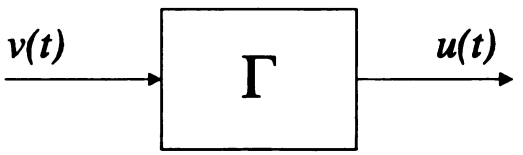

Figure 2.4: Schematic representation of a Preisach operator.

known. The memory curve indicates the dividing line between all hysterons with output $+1$ and with output -1. Given the initial memory curve, it is straightforward to obtain the memory curve at time t. Fig. 2.5 illustrates the general idea. The initial memory curve is labeled $M(t=0)$ in Fig. 2.5 (a). The input to the hysteron operator, v, at time $t=0$ is labeled v_0. The input will always be the point where the memory curve intersects the line $\beta = \alpha$. The memory curve divides the Preisach plane into two regions. Every hysteron whose (β, α) pair lies above or to the right (below or to the left) of the memory curve will have configuration -1 $(+1)$. If the input to the Preisach operator is then monotonically decreased to v_1 at time $t=1$, then the corresponding memory curve is $M(t=1)$ in Fig. 2.5 (b). Decreasing the input to any hysteron can only change the output of that hysteron if the β-level is crossed. This gives the vertical portion of the memory curve in $M(t=1)$; all of the hysterons to the right of the memory curve that were previously (in Fig. 2.5 (a)) configured as $+1$ have switched to -1 with their respective β-level crossings. Figs. 2.5 (c) and (d) show the memory curve when the output is increased monotonically to v_3 at time $t=3$, then increased monotonically to v_4 at time $t=4$. Since $v_4 > v_0$, the last increase removes all the corners from the memory curve when the output surpasses its uppermost portion. Combining any initial memory curve with any discretization, the lower and upper areas, C_k^+ and C_k^-, of each cell can be obtained by updating the memory curve as previously illustrated.

One more important property of the Preisach operators used in this thesis is that they are rate-independent. This means that the output of each hysteron and therefore the Preisach operator itself does not depend on the slope of the input. The parameter vector θ_H is invariant with regard to the input. In [2, 3], Tan and Baras show that for a specific

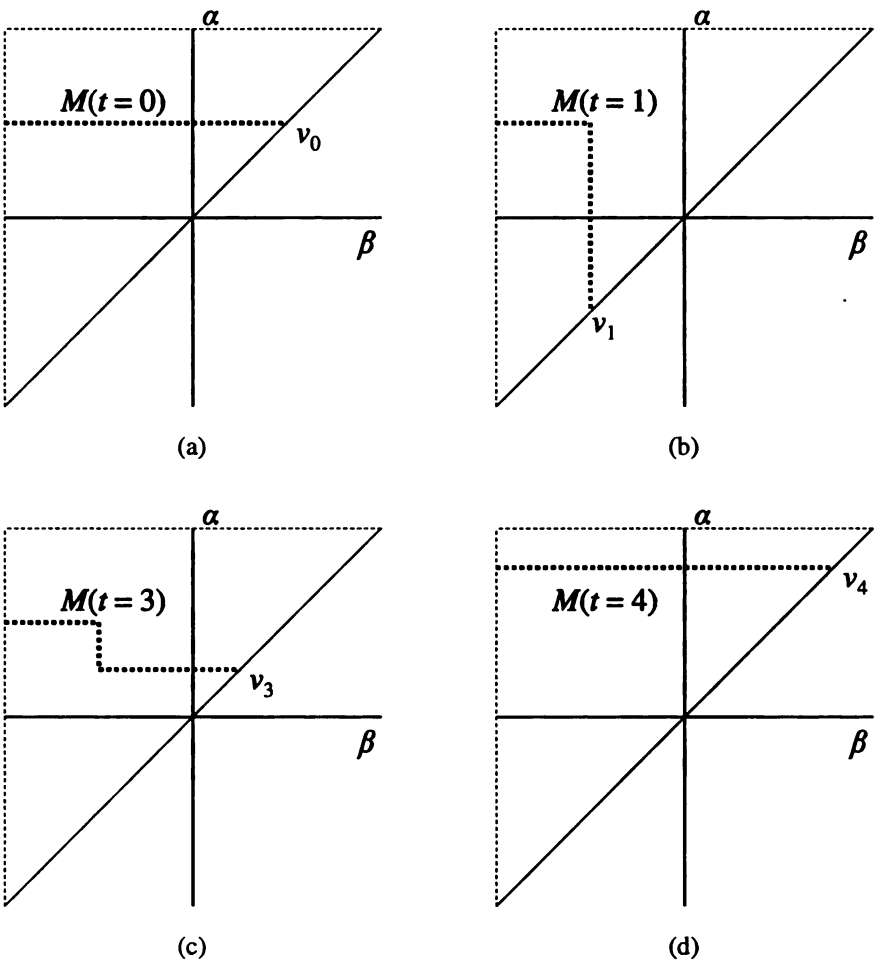

Figure 2.5: Evolution of the memory curve M with time.

actuator, rate-independence is a valid assumption for low input frequencies. They derive a dynamical model to approximate the rate-dependence at higher frequencies. In [6], the linear dynamics in cascade with the Preisach operator are shown to adequately capture the rate-dependent behavior of a given piezoelectric positioning scheme, which illustrates the motivation for both the Preisach operator (memory) and the linear dynamics (rate-dependence).

To summarize the previous section, the truncated Preisach operator is a way of approximating a hysteretic phenomenon. The output of a truncated Preisach operator can be expressed as the inner product of a time-varying regressor vector and a constant parameter

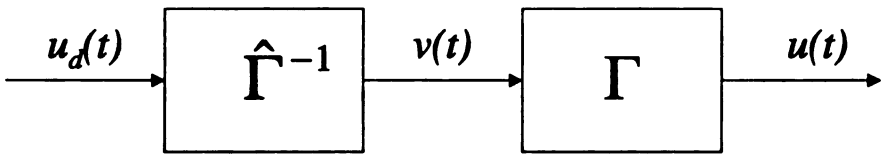

Figure 2.6: A Preisach operator and its approximate right inverse.

vector. The regressor vector is known if both the initial memory curve and the input of the Preisach operator are known. The memory curve can always be set to a known "initial" value by driving the input to the Preisach operator above α_{max} or below β_{min}.

2.2 *Inversion of the Preisach Operator*

The exact inverse of a discrete Preisach operator is a topic of the work in [3]. The algorithm for (exactly) inverting the Preisach operator is not of concern in this thesis, so additional information can be found therein. Certain relationships of a Preisach operator and its inverse are essential to the development in later sections.

The inversion algorithm in [3] will produce the exact "right" inverse of the Preisach operator (see Fig. 2.6) when the true parameter vector, θ_H is known. This gives

$$u(t) = \left(\Gamma \circ \Gamma^{-1}\right)(u_d(t)) = u_d(t).$$

From [6], if instead of the exact parameters, the inversion is based on a parameter estimate, $\hat{\theta}_H(t)$, then the inversion will result in

$$u_d(t) - u(t) = \left(\hat{\theta}_H(t) - \theta_H\right)^T w_H(t) = \tilde{\theta}_H^T w_H(t). \tag{2.10}$$

The Preisach inverse is a user-defined quantity with discretization level L. When used to (approximately) invert a Preisach operator with a continuous weighting function, rather than discrete, an error term is introduced to (2.10). The new relationship is

$$u_d(t) - u(t) = \tilde{\theta}_H^T w_H(t) + d_H(t), \tag{2.11}$$

where $d_H(t)$ is a bounded disturbance with bound established in [3]. The last equation is the same relationship as that for the piecewise linear hysteresis model in [5]. This means that the overparameterization method proposed by Tao and Kokotovic could be applied using a Preisach operator rather than the piecewise linear hysteresis model, if computational complexity were not an issue.

3. Problem Formulation

3.1 *System Error Dynamics*

The control scheme in this thesis uses multi-time scale slow adaptation to accommodate bilinearly coupled parameters without the use of overparameterization. The MRAC framework will be the same as in [5]. This work was first undertaken by Tan and Khalil [6] and continued by Reynolds, Tan and Khalil [11].

Let $G_p(s) = k_p \frac{Z_p(s)}{P_p(s)}$, where k_p is the high-frequency gain, $P_p(s)$ and $Z_p(s)$ are monic, coprime polynomials of degree n and m, respectively. The plant has state space representation $(A_p, B_p, C_p, 0)$ so that

$$\begin{aligned} \dot{x}_p(t) &= A_p x_p(t) + B_p u(t) \\ y(t) &= C_p x_p(t). \end{aligned} \tag{3.1}$$

The goal of the controller design is to make the plant output $y(t)$ track the reference output. The output of the model is given by $y_m(t) = G_m(s)[r](t)$, where $r(t)$ is a bounded, piecewise continuous reference input and $G_m(s)[r](t)$ is the time domain output of the transfer function $G_m(s)$ acting on the signal $r(t)$. The following assumptions, from [5, 6, 11], are made about the plant and reference model:

- **(A1)** $Z_p(s)$ is a stable polynomial;
- **(A2)** The degrees n and m are known;
- **(A3)** $k_p > 0$;
- **(A4)** The model, $G_m(s) = \frac{1}{P_m(s)}$, has stable polynomial $P_m(s)$ of degree $n^* = n - m$.

The proposed controller structure (shown in Fig. 3.1) consists of two parts: a classical MRAC that can be found in adaptive control texts such as [8, 12], and the Preisach inverse estimate, which will directly precede the actuator illustrated in Fig. 1.1.

With exact hysteresis cancellation and knowledge of the plant parameters, perfect

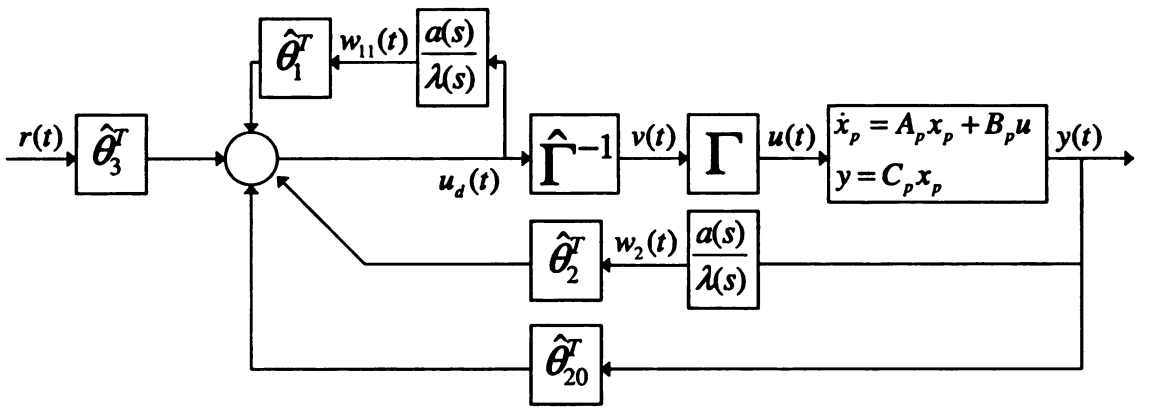

Figure 3.1: The proposed controller with parameter estimates.

model following can be achieved with

$$u(t) = \theta_1^T w_1(t) + \theta_2^T w_2(t) + \theta_{20} y(t) + \theta_3 r(t), \tag{3.2}$$

where

$$w_1(t) \triangleq \frac{a(s)}{\lambda(s)}[u](t),\ w_2(t) \triangleq \frac{a(s)}{\lambda(s)}[y](t),\ \frac{a(s)}{\lambda(s)} = \frac{1}{\lambda(s)} \begin{bmatrix} 1 \\ s \\ \vdots \\ s^{n-2} \end{bmatrix},$$

and $\lambda(s)$ is a stable polynomial of degree $n-1$. The parameters $\theta_1 \in \mathbb{R}^{n-1}$, $\theta_2 \in \mathbb{R}^{n-1}$, $\theta_{20} \in \mathbb{R}$ and $\theta_3 \in \mathbb{R}$ are determined by the matching equation:

$$\theta_1^T a(s) P_p(s) + \left[\theta_2^T a(s) + \theta_{20}\lambda(s)\right] k_p Z_p(s) = \lambda(s)\left[P_p(s) - \theta_3 k_p Z_p(s) P_m(s)\right]. \tag{3.3}$$

Now define a controllable canonical pair (Λ, B_λ) such that

$$(sI - \Lambda)^{-1} B_\lambda = \frac{a(s)}{\lambda(s)}. \tag{3.4}$$

Using (3.1) and (3.4), the state space form of the system with perfect matching is

$$\begin{aligned}
\dot{x}_{pm} &= A_p x_{pm} + B_p\left(\theta_1^T w_{m1} + \theta_2^T w_{m2} + \theta_{20} C_p x_{pm} + \theta_3 r\right) \\
\dot{w}_{m1} &= \Lambda w_{m1} + B_\lambda\left(\theta_1^T w_{m1} + \theta_2^T w_{m2} + \theta_{20} C_p x_{pm} + \theta_3 r\right) \\
\dot{w}_{m2} &= \Lambda w_{m2} + B_\lambda C_p x_{pm}.
\end{aligned}$$

The closed-loop form of the perfect model following equations are

$$\begin{bmatrix} \dot{x}_{pm} \\ \dot{w}_{m1} \\ \dot{w}_{m2} \end{bmatrix} = \begin{bmatrix} A_p + B_p\theta_{20}C_p & B_p\theta_1^T & B_p\theta_2^T \\ B_\lambda\theta_{20}C_p & \Lambda + B_\lambda\theta_1^T & B_\lambda\theta_2^T \\ B_\lambda C_p & 0 & \Lambda \end{bmatrix} \begin{bmatrix} x_{pm} \\ w_{m1} \\ w_{m2} \end{bmatrix} + \begin{bmatrix} B_p\theta_3 \\ B_\lambda\theta_3 \\ 0 \end{bmatrix} r.$$

This is a non-minimal realization of the model, $G_m(s)$, so

$$\begin{aligned}
A_m &\triangleq \begin{bmatrix} A_p + B_p\theta_{20}C_p & B_p\theta_1^T & B_p\theta_2^T \\ B_\lambda\theta_{20}C_p & \Lambda + B_\lambda\theta_1^T & B_\lambda\theta_2^T \\ B_\lambda C_p & 0 & \Lambda \end{bmatrix}, B_m \triangleq \begin{bmatrix} B_p\theta_3 \\ B_\lambda\theta_3 \\ 0 \end{bmatrix}, \\
C_m &\triangleq \begin{bmatrix} C_p & 0 & 0 \end{bmatrix}
\end{aligned}$$

are defined with appropriate dimensions, giving

$$\begin{aligned}
\dot{x}_m &= A_m x_m + B_m r \\
y_m &= C_m x_m,
\end{aligned}$$

where $x_m \triangleq [x_{pm}^T, w_{m1}^T, w_{m2}^T]^T$.

The signal $w_1(t)$ is unavailable because the output of the Preisach operator, $u(t)$, is unavailable. Since $w_1(t)$ and the true plant parameters are both unknown, the implemented

control is

$$u_d(t) = \hat{\theta}_1^T w_{11}(t) + \hat{\theta}_2^T w_2(t) + \hat{\theta}_{20} y(t) + \hat{\theta}_3 r(t), \tag{3.5}$$

where $\hat{\theta}_k$ is an estimate of θ_k and

$$w_{11}(t) \triangleq \frac{a(s)}{\lambda(s)}[u_d](t). \tag{3.6}$$

The true hysteresis parameters are also unknown, so the inversion will be performed based on estimates of those parameters. The following two assumptions are made about the hysteresis operator, Γ, and its approximate inverse, $\hat{\Gamma}^{-1}$:

- **(A5)** Γ is a Preisach operator with piecewise uniform weighting function characterized by $\theta_H \in \mathbb{R}^{n_H}$, as discussed in Sec. 2.2. Furthermore, the weights corresponding to each cell adjacent to the line $\alpha = \beta$ are nonzero;
- **(A6)** The inversion error $u_d - u$ satisfies (2.11);
- **(A7)** The control effort u_d remains (or is forced to remain) within the saturation limits corresponding to the output range of the Preisach operator.

The last assumption ensures that the finite-dimensional signal w_H can accurately model the internal state of the Preisach operator. If the control is unrestricted, than an infinite-dimensional w_H would be necessary to capture its effect, which is computationally infeasible and unnecessary for many true hysteretic systems. With the control signal u_d in (3.5) and (2.11), the system has the state space representation

$$\begin{aligned}
\dot{x}_p &= A_p x_p + B_p u = A_p x_p + B_p \left(u_d - \tilde{\theta}_H^T w_H - d_H\right) \\
&= A_p x_p + B_p \left(\hat{\theta}_1^T w_{11} + \hat{\theta}_2^T w_2 + \hat{\theta}_{20} C_p x_p + \hat{\theta}_3 r - \tilde{\theta}_H^T w_H - d_H\right) \\
\dot{w}_1 &= \Lambda w_1 + B_\lambda u = \Lambda w_1 + B_\lambda \left(u_d - \tilde{\theta}_H^T w_H - d_H\right) \\
&= \Lambda w_1 + B_\lambda \left(\hat{\theta}_1^T w_{11} + \hat{\theta}_2^T w_2 + \hat{\theta}_{20} C_p x_p + \hat{\theta}_3 r - \tilde{\theta}_H^T w_H - d_H\right) \\
\dot{w}_2 &= \Lambda w_2 + B_\lambda C_p x_p.
\end{aligned}$$

Now, using (2.11), substituting $\hat{\theta}_k = \tilde{\theta}_k + \theta_k$ and adding and subtracting $\hat{\theta}_1^T w_1$, the closed-loop state model becomes

$$\begin{bmatrix} \dot{x}_p \\ \dot{w}_1 \\ \dot{w}_2 \end{bmatrix} = A_m \begin{bmatrix} x_p \\ w_1 \\ w_2 \end{bmatrix} + \frac{B_m}{\theta_3}\left(\tilde{\theta}_1^T w_1 + \tilde{\theta}_2^T w_2 + \tilde{\theta}_{20} C_p x_p + \hat{\theta}_3 r + \hat{\theta}_1^T (w_{11} - w_1) - \tilde{\theta}_H^T w_H - d_H\right). \tag{3.7}$$

The error state is defined as

$$e_1 = \begin{bmatrix} e_{11} \\ e_{12} \\ e_{13} \end{bmatrix} \triangleq \begin{bmatrix} x_p - x_{pm} \\ w_1 - w_{m1} \\ w_2 - w_{m2} \end{bmatrix},$$

and subtracting (3.5) from (3.7), the error dynamics become

$$\dot{e}_1 = A_m e_1 + \frac{B_m}{\theta_3}\left(\tilde{\theta}_1^T w_1 + \tilde{\theta}_2^T w_2 + \tilde{\theta}_{20} C_p x_p + \tilde{\theta}_3 r + \hat{\theta}_1^T (w_{11} - w_1) - \tilde{\theta}_H^T w_H - d_H\right). \tag{3.8}$$

The driving terms on the right-hand side of (3.8) are dependent on the error state, so each much be separated into internal and exogeneous parts,

$$\begin{bmatrix} r \\ C_p x_p \\ w_1 \\ w_2 \end{bmatrix} = \begin{bmatrix} r \\ C_p (x_p - x_{pm} + x_{pm}) \\ w_1 - w_{m1} + w_{m1} \\ w_2 - w_{m2} + w_{m2} \end{bmatrix} = \begin{bmatrix} r \\ C_p (e_{11} + x_{pm}) \\ e_{12} + w_{m1} \\ e_{13} + w_{m2} \end{bmatrix}.$$

The closed-loop dynamics now become

$$\dot{e}_1 = \left[A_m + \frac{B_m}{\theta_3}\left(\tilde{\theta}_G^T Q\right)\right] e_1 + \frac{B_m}{\theta_3}\left(\tilde{\theta}_3 r + \tilde{\theta}_G^T w_m + \hat{\theta}_1^T (w_{11} - w_1) - \tilde{\theta}_H^T w_H - d_H\right), \tag{3.9}$$

where

$$\tilde{\theta}_G \triangleq \begin{bmatrix} \tilde{\theta}_{20} \\ \tilde{\theta}_1 \\ \tilde{\theta}_2 \end{bmatrix}, \; w_m(t) \triangleq \begin{bmatrix} C_p x_m(t) \\ w_{m1}(t) \\ w_{m2}(t) \end{bmatrix}, \; Q \triangleq \begin{bmatrix} C_p & 0 & 0 \\ 0 & I & 0 \\ 0 & 0 & I \end{bmatrix}, \tag{3.10}$$

$C_p \in \mathbb{R}^{1\times n}$, $I \in \mathbb{R}^{n-1\times n-1}$ is the identity matrix and the remaining dimensions are defined appropriately. Notice that the quantity $w_{11} - w_1$ is left alone, as it depends on the hysteresis parameter error, not the error state e_1. In particular,

$$w_{11}(t) - w_1(t) = \frac{a(s)}{\lambda(s)}[u_d](t) - \frac{a(s)}{\lambda(s)}[u](t) = \frac{a(s)}{\lambda(s)}[\tilde{\theta}_H^T w_H + d_H](t). \tag{3.11}$$

From this point forward we make the following assumption, so that conclusions on parameter convergence can be drawn:

- **(A8)** The bounded disturbance, $d_H(t)$, is identically zero, i.e. $d_H(t) = 0 \;\; \forall\, t$.

3.2 *Uniqueness of the Solution*

It is shown by Sastry and Bodson in [8] that the matching equation (3.3) has a unique set of parameters $\{\theta_1, \theta_2, \theta_{20}, \theta_3\}$ by which it is satisfied. For this case, with a Preisach operator and its right inverse preceding the linear dynamics $G_p(s)$, it will now be shown that there are in fact an infinite number of solutions that produce the same input to the linear dynamics, and therefore produce the same ideal output $y_m(t)$.

Consider the case when the exact Preisach inverse is known, and the problem reduces to a classical MRAC. The control signal that gives asymptotic tracking of the reference model then is given in (3.2) as

$$u(t) = \theta_1^T w_1(t) + \theta_2^T w_2(t) + \theta_{20} y(t) + \theta_3 r(t).$$

This is the case when all parameter errors (plant and hysteresis) are zero. Now instead

consider the case

$$\begin{bmatrix} \hat{\theta}_1 \\ \hat{\theta}_2 \\ \hat{\theta}_{20} \\ \hat{\theta}_3 \\ \hat{\theta}_H \end{bmatrix} = \begin{bmatrix} \theta_1 \\ a\theta_2 \\ a\theta_{20} \\ a\theta_3 \\ a\theta_H \end{bmatrix} \Rightarrow \begin{bmatrix} \tilde{\theta}_1 \\ \tilde{\theta}_2 \\ \tilde{\theta}_{20} \\ \tilde{\theta}_3 \\ \tilde{\theta}_H \end{bmatrix} = \begin{bmatrix} 0 \\ (a-1)\,\theta_2 \\ (a-1)\,\theta_{20} \\ (a-1)\,\theta_3 \\ (a-1)\,\theta_H \end{bmatrix} \tag{3.12}$$

for some constant $a \neq 0$. Note that

$$u_d(t) - u(t) = \tilde{\theta}_H^T w_H(t) = (a-1)\,\theta_H^T w_H(t) = (a-1)\,u(t) \Rightarrow u_d(t) = au(t).$$

Using (2.10) and substituting the values from (3.12) the control signal applied to the plant is

$$\begin{aligned} u(t) &= u_d(t) - \tilde{\theta}_H^T w_H(t) \\ &= \hat{\theta}_1^T \frac{a(s)}{\lambda(s)}\,[u_d]\,(t) + \hat{\theta}_2^T w_2(t) + \hat{\theta}_{20} y(t) + \hat{\theta}_3 r(t) - \tilde{\theta}_H^T w_H(t) \\ &= \theta_1^T \frac{a(s)}{\lambda(s)}\,[au]\,(t) + a\theta_2^T w_2(t) + a\theta_{20} y(t) + a\theta_3 r(t) - (a-1)u(t) \\ au(t) &= a\left(\theta_1^T w_1(t) + \theta_2^T w_2(t) + \theta_{20} y(t) + \theta_3 r(t)\right), \end{aligned} \tag{3.13}$$

and eliminating the factor a from both sides of (3.13) gives the same control signal as in (3.2). Notice that although there are an infinite number of solutions, the value of $\hat{\theta}_1$ is the same in all of them. In order to overcome the issue of ambiguity of multiple equivalent solutions, and observe convergence of the parameter error to zero, the reference signal gain $\hat{\theta}_3$ will be set to a fixed value. This will ensure that there is again a unique set of parameter estimates that produces asymptotic tracking. To simplify the notation, it will be assumed that $\hat{\theta}_3 = \theta_3 = \frac{1}{k_p}$, as derived in [8]. This way all of the true plant parameter values do not change from those found by the matching equation (3.3) and the true hysteresis parameter

values θ_H reflect the true gain of the Preisach operator. Setting the parameter estimate $\hat{\theta}_3$ to its true value is merely a convention; if instead $\hat{\theta}_3$ were some scaled version of θ_3 (e.g. $\hat{\theta}_3 \equiv 1$), the aforementioned parameter values would be scaled accordingly as in (3.12) (by a factor of $a = \frac{1}{\theta_3}$).

Having established $\tilde{\theta}_3 \equiv 0$, (3.9) can now be simplified to

$$\dot{e}_1 = \left[A_m + \frac{B_m}{\theta_3}\left(\tilde{\theta}_G^T Q\right)\right] e_1 + \frac{B_m}{\theta_3}\left(\tilde{\theta}_G^T w_m + \hat{\theta}_1^T (w_{11} - w_1) - \tilde{\theta}_H^T w_H\right). \tag{3.14}$$

3.3 *Adaptation Rules*

With the error dynamics defined, the parameter estimate dynamics will now be derived. The adaptation rule is chosen using a gradient update law, which minimizes $\frac{1}{2}(C_m e_1)^2 = \frac{1}{2}(y - y_m)^2$. The adaptation rule is

$$\dot{\hat{\theta}} = -\begin{bmatrix} \Gamma_G & 0 \\ 0 & \Gamma_H \end{bmatrix} C_m e_1 \frac{\partial (C_m e_1)}{\partial \hat{\theta}} \tag{3.15}$$

where

$$\hat{\theta} \triangleq \begin{bmatrix} \hat{\theta}_G \\ \hat{\theta}_H \end{bmatrix},$$

and where $\Gamma_G \in \mathbb{R}^{2n-1 \times 2n-1}$, $\Gamma_H \in \mathbb{R}^{n_H \times n_H}$ are diagonal matrices with positive coefficients, γ_G and $\gamma_H = \gamma_G \gamma'$, respectively. Note that $\hat{\theta}_G = \tilde{\theta}_G + \theta_G$ and $\hat{\theta}_H = \tilde{\theta}_H + \theta_H$ are the estimates of the plant and hysteresis parameters, respectively. Applying the adaptation rule (3.15) to the error dynamics (3.14) gives the following adaptation law:

$$\dot{\hat{\theta}} = -\gamma_G C_m e_1 G_m \left(\begin{bmatrix} C_p x_p \\ w_{11} \\ w_2 \\ \gamma' \left(\left(\frac{a(s)}{\lambda(s)} [w_H^T] \right)^T \hat{\theta}_1 - w_H \right) \end{bmatrix} \right), \tag{3.16}$$

where $G_m([z(\cdot)])$ is the output of $G_m(s)$ acting component-wise on the input vector $z(\cdot)$, $0 < \gamma_G << 1$ separates the error dynamics and adaptation into two time scales, and $0 < \gamma' << 1$ further separates the adaptation of the plant and hysteresis parameters into two time scales. Notice that applying the gradient update law (3.15) to (3.8) gives a factor of $\frac{1}{\theta_3}$. By (**A3**) this can be absorbed into the adaptation gain. All of the signals in (3.16) are available online. The true parameters θ are taken as constant, so $\dot{\hat{\theta}} = \dot{\tilde{\theta}}$. As in the case of error dynamics, the parameter update law will be expressed in terms of error e_1 and driving signals.

$$\dot{\hat{\theta}} = -\gamma_G C_m e_1 G_m \left(\begin{bmatrix} w_m \\ 0 \end{bmatrix} + \begin{bmatrix} Qe_1 \\ 0 \end{bmatrix} + \begin{bmatrix} 0 \\ w_{11} - w_1 \\ 0 \\ \gamma' \left(\left(\frac{a(s)}{\lambda(s)} [w_H^T] \right)^T \hat{\theta}_1 - w_H \right) \end{bmatrix} \right) \tag{3.17}$$

Equations (3.14) and (3.17) now give a complete expression for the closed-loop dynamics. From this point on, $\overline{w}_H(t)$ will be considered the approximation of $w_H(t)$ when the states are near the origin, i.e. $\overline{w}_H(t) = w_H(t)\ \forall\, t \geq 0$ if $e_1(t) = 0,\ \tilde{\theta}(t) = 0,\ \forall\, t \geq 0$. Now make the following assumption:

- **(A9)** The signal $\overline{w}_H(t)$ is bounded and continuous.

This assumption is not stringent, provided the input to the Preisach operator is bounded and continuous. Using the fact that $(e_1^T,\ \tilde{\theta}^T) = 0$ is an equilibrium point of (3.14) and (3.17), a local approximation of the dynamics near the origin will be derived, so that local results can be obtained. Establishing the stability of the approximate system is useful for establishing the stability of the origin of the complete nonlinear system, at least in some neighborhood of the true parameter values. The approximate dynamics in the neighborhood of $(e_1^T,\ \tilde{\theta}^T) = 0$ are found by linearizing (3.14) and (3.17) after substituting $\overline{w}_H(t)$

for $w_H(t)$. The results are

$$\begin{aligned}
\dot{e}_1 &= A_m e_1 + \frac{B_m}{\theta_3}\left(\tilde{\theta}^T \begin{bmatrix} w_m \\ \left(\frac{a(s)}{\lambda(s)}[\overline{w}_H^T]\right)^T \theta_1 - \overline{w}_H \end{bmatrix}\right) \\
\dot{\tilde{\theta}} &= -\gamma_G C_m e_1 G_m \left(\begin{bmatrix} w_m \\ \gamma'\left(\left(\frac{a(s)}{\lambda(s)}[\overline{w}_H^T]\right)^T \theta_1 - \overline{w}_H\right) \end{bmatrix}\right).
\end{aligned}$$

Since the right-hand side now only depends linearly on e_1 and $\tilde{\theta}$, a new signal is defined

$$\overline{w}_{HF} \triangleq \left(\frac{a(s)}{\lambda(s)}[\overline{w}_H^T]\right)^T \theta_1 - \overline{w}_H,$$

so that the approximate linear dynamics take the final form

$$\dot{e}_1 = A_m e_1 + \frac{B_m}{\theta_3}\left(\tilde{\theta}^T \begin{bmatrix} w_m \\ \overline{w}_{HF} \end{bmatrix}\right) \tag{3.18}$$

$$\dot{\tilde{\theta}} = -\gamma_G C_m e_1 G_m \left(\begin{bmatrix} w_m \\ \gamma'\overline{w}_{HF} \end{bmatrix}\right). \tag{3.19}$$

In Section 4.3, the validity of this approximation method will be discussed.

4. Averaging Analysis

4.1 *An Identification Problem*

In [6], Tan and Khalil present an identification problem containing both linear and bilinearly coupled parameters, as in the closed-loop error dynamics in (3.14)[1]. This first step in the system analysis has promising results, and is repeated here to motivate further analysis. Consider the error

$$e_z(t) = \hat{z}(t) - z(t) \tag{4.1}$$

and corresponding signals

$$z(t) = \theta_a^T w_a(t) + \theta_b^T G_b(s)\left[\theta_a^T w_a\right](t) \tag{4.2}$$

$$\hat{z}(t) = \hat{\theta}_a^T w_a(t) + \hat{\theta}_b^T G_b(s)\left[\hat{\theta}_a^T w_a\right](t), \tag{4.3}$$

where $\theta_a \in \mathbb{R}^{n_a}$, $w_a \in \mathbb{R}^{n_a}$, $\theta_b \in \mathbb{R}^{n_b}$ and $G_b(s)$ is a stable transfer function with dimension n_b. In the original paper there is also a scalar transfer function operating on the right hand side of both equations. This transfer function is omitted here because it is shown therein that the transfer function does not complicate the analysis when slow adaptation is implemented and the time scales of the parameter adaptation and the transfer function are sufficiently separated. The parameter adaptation rules are

$$\dot{\hat{\theta}}_a = -\gamma_a e_z \left(w_a + G_b(s)\left[w_a^T\right]\theta_b\right) \tag{4.4}$$

$$\dot{\hat{\theta}}_b = -\gamma_b e_z G_b(s)\left[\hat{\theta}_a^T w_a\right], \tag{4.5}$$

[1] In order to clearly see the bilinearly coupled parameters in (3.14), one can make a substitution using (3.11).

where $0 < \gamma_a << \gamma_b << 1$. To simplify the notation, assume $n_b = 1$. The following matrices

$$\begin{aligned}
\overline{AA^T} &\triangleq \text{avg}\left(w_a(t)w_a^T(t)\right), \\
\overline{BB^T} &\triangleq \text{avg}\left(G_b(s)\left[w_a\right](t)G_b(s)\left[w_a^T(t)\right]\right), \\
\overline{AB^T} &\triangleq \text{avg}\left(w_a(t)G_b(s)\left[w_a^T(t)\right]\right), \\
\overline{BA^T} &\triangleq \text{avg}\left(G_b(s)\left[w_a\right](t)w_a^T(t)\right), \\
\overline{(A+\theta_b B)B^T} &\triangleq \overline{AB^T} + \theta_b \overline{BB^T}, \\
\overline{(A+\theta_b B)^2} &\triangleq \text{avg}\left(\left(w_a(t) + \theta_b G_b(s)\left[w_a\right](t)\right)\left(w_a(t) + \theta_b G_b(s)\left[w_a\right](t)\right)^T\right)
\end{aligned}$$

are assumed to exist for arbitrary t_0, where $\text{avg}(\cdot) = \lim_{T\to\infty} \frac{1}{T}\int_{t_0}^{t_0+T}(\cdot)dt$. For T-periodic regressor $w_a(t)$, all of the matrices are guaranteed to exist. Theorem 5.1 of [6] states that for the system with error dynamics (4.1)-(4.3) and adaptation rules (4.4) and (4.5), if

$$\theta_a^T \overline{BB^T}\theta_a > 0 \tag{4.6}$$

$$\overline{(A+\theta_b B)^2} - \frac{\overline{(A+\theta_b B)B^T}\theta_a\theta_a^T\overline{(A+\theta_b B)B^T}^T}{\theta_a^T\overline{BB^T}\theta_a} > 0 \tag{4.7}$$

and if $\hat{\theta}_a(t=0)$ is sufficiently close to then θ_a all parameter estimates will converge to their true values. The proof is straightforward and uses averaging analyses and linearization of the slow dynamics. This will give zero output error and complete knowledge of the system parameters.

4.2 *The Local Approximate Closed-Loop System*

The identification problem in Section 4.1 is a good motivational example, but the most interesting aspect of the problem is the behavior of the closed-loop system. In the closed-loop control case, the regressor vectors cannot be arbitrarily chosen. They will depend on feedback, and the regressor $w_H(t)$ depends nonlinearly on internal signals, as

discussed in Section 3.3. Nonlinear analysis of the closed-loop system has not been thoroughly completed, but analysis of the approximate system in a sufficiently small neighborhood of zero parameter error is presented. These results are then used to construct a converse Lyapunov function and show local stability of the true closed-loop system dynamics.

Two-time scale averaging theory is now applied to the approximate system dynamics given in (3.18) and (3.19). Equation (3.18) is the fast state, while (3.19) is the slow state, as dictated by the adaptation gain γ_G. The steady-state value of e_1 with the parameter estimate error $\tilde{\theta}$ frozen is

$$v(t,\tilde{\theta}) \triangleq \int_0^t e^{A_m(t-\tau)} \frac{B_m}{\theta_3} \left[w_m^T,\ \overline{w}_{HF}^T\right] d\tau \tilde{\theta}.$$

The function

$$f'(t,\tilde{\theta},v) \triangleq C_m v G_m \left(\begin{bmatrix} w_m \\ \gamma' \overline{w}_{HF} \end{bmatrix} \right)$$

is defined for more compact notation. These assumptions are made:

- **(B1)**

$$F_{av} \triangleq \lim_{T\to\infty} \frac{1}{T} \int_{t_0}^{t_0+T} \left(G_m \left(\begin{bmatrix} w_m \\ \gamma' \overline{w}_{HF} \end{bmatrix} \right) C_m \int_0^t e^{A_m(t-s)} \frac{B_m}{\theta_3} \left[w_m^T,\ \overline{w}_{HF}^T\right] ds \right) dt$$

  exists uniformly in t_0.

- **(B2)**

$$\frac{\partial f'(t,\tilde{\theta},v)}{\partial \tilde{\theta}} - F_{av}$$

  has zero average value, with convergence function $\zeta(T)$, where $\zeta(\cdot) : \mathbb{R}_+ \to \mathbb{R}_+$ is strictly decreasing and

$$\left\| \frac{1}{T} \int_{t_0}^{t_0+T} f'(\tau,\tilde{\theta},v)\, d\tau - F_{av} \right\| \leq \zeta(T)$$

Theorem 4.1 *Consider the error dynamics (3.18) and the adaptation rule (3.19). If assumptions* (**B1**)-(**B2**) *are satisfied, and* $\bar{\tilde{\theta}} = 0$ *is an exponentially stable equilibrium point of the averaged system,*

$$\dot{\bar{\tilde{\theta}}} = -\gamma_G F_{av} \bar{\tilde{\theta}} \tag{4.8}$$

then ($e_1 = 0$, $\tilde{\theta} = 0$) *is an exponentially stable equilibrium of the system (3.18)-(3.19) for* γ_G *sufficiently small.*

Proof. From its structure, $f'(t, \tilde{\theta}, v)$ is locally Lipschitz in $(\tilde{\theta}, v)$. Moreover, since w_m and $\overline{w}_{HF}$ are piecewise continuous in t and bounded, f' is continuous in t. Define

$$h(t, \tilde{\theta}) \triangleq \frac{B_m}{\theta_3} \left(\tilde{\theta}^T \begin{bmatrix} w_m \\ \overline{w}_{HF} \end{bmatrix} \right).$$

Clearly, $h(t,0) = 0$ for all $t > 0$ and $\left\| \frac{\partial h(t,\tilde{\theta})}{\partial \tilde{\theta}} \right\|$ is bounded for all $t > 0$. Combining the above and assumptions (**B1**)-(**B2**), the conditions of Theorem 4.4.3 of [8] are satisfied. □

It remains to be shown that $\bar{\tilde{\theta}} = 0$ is an exponentially stable equilibrium of the averaged system. The averaged system is given by (4.8). Notice that

$$C_m v\left(t, \bar{\tilde{\theta}}\right) = \frac{1}{\theta_3} G_m\left(\left[w_m^T, \overline{w}_{HF}^T\right]\right) \bar{\tilde{\theta}}.$$

By assumption (**B1**), these quantities all exist,

$$\overline{MM^T} \triangleq \operatorname{avg}\left(G_m([w_m]) G_m\left([w_m^T]\right)\right), \tag{4.9}$$

$$\overline{HH^T} \triangleq \operatorname{avg}\left(G_m([\overline{w}_{HF}]) G_m\left([\overline{w}_{HF}^T]\right)\right), \tag{4.10}$$

$$\overline{MH^T} \triangleq \operatorname{avg}\left(G_m([w_m]) G_m\left([\overline{w}_{HF}^T]\right)\right), \tag{4.11}$$

$$\overline{HM^T} \triangleq \operatorname{avg}\left(G_m([\overline{w}_{HF}]) G_m\left([w_m^T]\right)\right). \tag{4.12}$$

Substituting the above quantities into (4.8) the averaged dynamics are

$$\dot{\bar{\tilde{\theta}}} = -\frac{\gamma_G}{\theta_3}\begin{bmatrix} \overline{MM^T} & \overline{MH^T} \\ \gamma'\overline{HM^T} & \gamma'\overline{HH^T} \end{bmatrix}\bar{\tilde{\theta}} \tag{4.13}$$

Within the averaged system, the parameter estimate dynamics can be further separated into two time scales. The averaged dynamics, separated by time scales, are

$$\dot{\bar{\tilde{\theta}}}_H = -\frac{\gamma_G\gamma'}{\theta_3}\left(\overline{HH^T}\bar{\tilde{\theta}}_H + \overline{HM^T}\bar{\tilde{\theta}}_G\right) \tag{4.14}$$

$$\dot{\bar{\tilde{\theta}}}_G = -\frac{\gamma_G}{\theta_3}\left(\overline{MH^T}\bar{\tilde{\theta}}_H + \overline{MM^T}\bar{\tilde{\theta}}_G\right), \tag{4.15}$$

where $\bar{\tilde{\theta}}_G$ and $\bar{\tilde{\theta}}_H$ are the averaged parameter estimate vectors. As a result of averaging, the system (4.14)-(4.15) is autonomous, and a two-time scale, slow and fast manifold analysis [13] can be performed. The system will be transformed into the slow time scale, $\tau = (\gamma_G\gamma'/\theta_3)t$, for convenience:

$$\frac{\partial\bar{\tilde{\theta}}_H}{\partial\tau} = -\left(\overline{HH^T}\bar{\tilde{\theta}}_H + \overline{HM^T}\bar{\tilde{\theta}}_G\right) \tag{4.16}$$

$$\gamma'\frac{\partial\bar{\tilde{\theta}}_G}{\partial\tau} = -\left(\overline{MH^T}\bar{\tilde{\theta}}_H + \overline{MM^T}\bar{\tilde{\theta}}_G\right). \tag{4.17}$$

The parameter γ' dictates that the state vector $\bar{\tilde{\theta}}_G$ is the fast state and that $\bar{\tilde{\theta}}_H$ is the slow state.

Theorem 4.2 (Theorem 3.1 from [9]) *Define the slow and fast system matrices as*

$$\Omega_s \triangleq \left(\overline{HH^T} - \overline{HM^T}\left(\overline{MM^T}\right)^{-1}\overline{MH^T}\right) \tag{4.18}$$

$$\Omega_f \triangleq \left(\overline{MM^T}\right). \tag{4.19}$$

If $\left(\overline{MM^T}\right)^{-1}$ *exists, then as* $\gamma' \to 0$ *the first* n_H *eigenvalues of the system (4.16)-(4.17) tend*

to positions in the complex plane defined by the eigenvalues of Ω_s, namely,

$$\lambda_i(\Omega_s), \quad i = 1,2,\ldots,n_H; \tag{4.20}$$

while the remaining $2n-1$ eigenvalues of the system (4.16)-(4.17) tend to infinity, with the rate of $1/\gamma'$, along asymptotes defined by the eigenvalues of Ω_f, namely

$$\frac{1}{\gamma'}\lambda_j(\Omega_f), \quad j = 1,2,\ldots,2n-1. \tag{4.21}$$

Furthermore, if the n_H eigenvalues of Ω_s are distinct and the $2n-1$ eigenvalues of Ω_f are distinct, where $\lambda_i(\Omega_s) = \lambda_j(\Omega_f)$ is allowed, then the eigenvalues of the original system (4.16)-(4.17) are approximated as

$$\lambda_i = \lambda_i(\Omega_s) + O(\gamma'), \quad i = 1,2,\ldots,n_H; \tag{4.22}$$

$$\lambda_i = \frac{\lambda_j(\Omega_f) + O(\gamma')}{\gamma'}, \quad i = n_H + j, \ j = 1,2,\ldots,2n-1, \tag{4.23}$$

where $O(\gamma')$ denotes a term on the order of magnitude of γ'.

Equations (4.16), (4.17), (4.18) and (4.19) are well known in singular perturbation analysis of linear systems [9]. Using the results of Theorem 4.2 in Theorem 4.1 shows that the origin ($e_1 = 0$, $\tilde{\theta} = 0$) is an exponentially stable equilibrium point of the approximated system, (3.18)-(3.19), provided that both Ω_f and Ω_s are positive definite (PD) and γ' is sufficiently small. The next theorem shows that (4.19) being PD is not a stringent condition.

Theorem 4.3 *Consider the matrix*

$$\Omega_s = \overline{HH^T} - \overline{HM^T}\left(\overline{MM^T}\right)^{-1}\overline{MH^T} \tag{4.24}$$

where $\overline{HH^T} \in \mathbb{R}^{n_H \times n_H}$, $\overline{HM^T} \in \mathbb{R}^{n_H \times 2n-1}$, $\overline{MH^T} \in \mathbb{R}^{2n-1 \times n_H}$ *and* $\overline{MM^T} \in \mathbb{R}^{2n-1 \times 2n-1}$ *are defined as in equations (4.9) through (4.12). Then, for all* $x \in \mathbb{R}^{n_H} \neq 0$, $x^T \Omega_s x \geq 0$.

Proof. Choose $x \in \mathbb{R}^{nH}$. Since the vector x is a constant, it can be moved inside the integral present in the averaging, i.e.

$$x^T \left[\lim_{T \to \infty} \frac{1}{T} \int_{t_0}^{t_0+T} (\cdot) dt \right] x = \lim_{T \to \infty} \frac{1}{T} \int_{t_0}^{t_0+T} x^T (\cdot) x dt.$$

Let avg $\left(x^T HH^T x\right)$, avg $\left(x^T HM^T\right)$ and avg $\left(MH^T x\right)$ be denoted $\overline{h^2}$, $\overline{hM^T}$ and $\overline{Mh}$, respectively. This gives

$$x^T \Omega_s x = \overline{h^2} - \overline{hM^T} \left(\overline{MM^T}\right)^{-1} \overline{Mh}. \tag{4.25}$$

It is easy to show for $z \in \mathbb{R}^n$ and $A = A^T \in \mathbb{R}^{n \times n}$, $z^T A z = \text{trace}\left[zz^T A\right]$, so we have

$$x^T \Omega_s x = \overline{h^2} - \text{trace}\left[\overline{Mh}\, \overline{hM^T} \left(\overline{MM^T}^{-1}\right)\right].$$

Notice that zz^T is a singular matrix with rank 1, which implies that for a full rank matrix A, $zz^T A$ is also a singular matrix with rank 1. Therefore we have

$$\overline{h^2} - \text{trace}\left[\overline{Mh}\, \overline{hM^T} \left(\overline{MM^T}^{-1}\right)\right] = \overline{h^2} - \lambda_{\max}\left[\overline{Mh}\, \overline{hM^T} \left(\overline{MM^T}^{-1}\right)\right].$$

From [14] p. 318,

$$\overline{h^2} - \lambda_{\max}\left[\overline{Mh}\, \overline{hM^T} \left(\overline{MM^T}^{-1}\right)\right] = \overline{h^2} - \max_{y \in \mathbb{R}^{2n-1} \setminus \{0\}} \left\{ \frac{y^T \overline{Mh}\, \overline{hM^T} y}{y^T \overline{MM^T} y} \right\}.$$

Now if one considers the averaging operator as an inner product and using the *Cauchy-Schwarz Inequality*,

$$\begin{aligned} \overline{h^2} - \max_{y \in \mathbb{R}^{2n-1} \setminus \{0\}} \left\{ \frac{y^T \overline{Mh}\, \overline{hM^T} y}{y^T \overline{MM^T} y} \right\} &\geq \overline{h^2} - \overline{h^2} \left(\max_{y \in \mathbb{R}^{2n-1} \setminus \{0\}} \left\{ \frac{y^T \overline{MM^T} y}{y^T \overline{MM^T} y} \right\} \right) \\ &= \overline{h^2} - \overline{h^2} = 0. \end{aligned} \tag{4.26}$$

Taking the first equation (4.25) and last inequality (4.26), it is clear that $x^T \Omega_s x \geq 0$. □

4.3 *Local Lyapunov Stability*

In the previous section, it was shown that the approximate local system has an exponentially stable equilibrium point at the origin. In order to rigorously show that this analysis implies exponential stability of the nonlinear system, a Lyapunov function will be constructed. Theorems 4.1 and 4.2 together state that for the approximate local system

$$\begin{bmatrix} \dot{e}_1 \\ \dot{\tilde{\theta}} \end{bmatrix} = \begin{bmatrix} A_m & \frac{B_m}{\theta_3} \begin{bmatrix} w_m^T & \overline{w}_{HF}^T \end{bmatrix} \\ -\gamma_G \int_0^t e^{A_m(t-\tau)} B_m \begin{bmatrix} w_m \\ \gamma' \overline{w}_{HF} \end{bmatrix} d\tau C_m & 0 \end{bmatrix} \begin{bmatrix} e_1 \\ \tilde{\theta} \end{bmatrix}, \quad (4.27)$$

$(e_1^T,\ \tilde{\theta}^T) = 0$ is exponentially stable. These quantities are defined for future use:

$$\begin{aligned} w_{HF} &\triangleq \left(\frac{a(s)}{\lambda(s)} [w_H^T] \right)^T \hat{\theta}_1 - w_H \\ \tilde{w}_{HF} &\triangleq \left(\frac{a(s)}{\lambda(s)} [w_H^T - \overline{w}_H^T] \right)^T \theta_1 - (w_H - \overline{w}_H) \end{aligned}$$

Equation (4.27) is the local approximation of

$$\begin{aligned} \dot{e}_1 &= \left[A_m + \frac{B_m}{\theta_3} \left(\tilde{\theta}_G^T Q \right) \right] e_1 + \frac{B_m}{\theta_3} \left(\tilde{\theta}_G^T w_m + \hat{\theta}_1^T (w_{11} - w_1) - \tilde{\theta}_H^T w_H \right), \\ \dot{\hat{\theta}} &= -\gamma_G C_m e_1 G_m \left(\begin{bmatrix} C_p x_p \\ w_{11} \\ w_2 \\ \gamma' w_{HF} \end{bmatrix} \right), \end{aligned} \quad (4.28)$$

a so-called *functional differential equation* (FDE). Recall that the signal w_{HF} is a function of the infinite-dimensional history of the state $(e_1^T,\ \tilde{\theta}^T)$ and $\overline{w}_{HF}$ is the model version of this signal, i.e. how the signal evolves when the true system parameters are known and the

state is identically zero. Adding and subtracting convenient terms to the right-hand side of (4.28) gives

$$\begin{aligned}
\begin{bmatrix} \dot{e}_1 \\ \dot{\tilde{\theta}} \end{bmatrix} &= \begin{bmatrix} A_m & \frac{B_m}{\theta_3}\begin{bmatrix} w_m^T & \overline{w}_{HF}^T \end{bmatrix} \\ -\gamma_G \int_0^t C_m e^{A_m(t-\tau)} B_m \begin{bmatrix} w_m \\ \gamma' \overline{w}_{HF} \end{bmatrix} d\tau C_m & 0 \end{bmatrix} \begin{bmatrix} e_1 \\ \tilde{\theta} \end{bmatrix} \\
&+ \begin{bmatrix} 0 & \frac{B_m}{\theta_3}\begin{bmatrix} 0^T & \tilde{w}_{HF}^T \end{bmatrix} \\ -\gamma_G \int_0^t e^{A_m(t-\tau)} B_m \begin{bmatrix} 0 \\ \gamma' \tilde{w}_{HF} \end{bmatrix} d\tau C_m & 0 \end{bmatrix} \begin{bmatrix} e_1 \\ \tilde{\theta} \end{bmatrix} \\
&+ \begin{bmatrix} \frac{B_m}{\theta_3}\left(\tilde{\theta}_G^T Q e_1 + \hat{\theta}_1^T \frac{a(s)}{\lambda(s)}\left[\tilde{\theta}_H^T w_H\right] - \theta_1^T \frac{a(s)}{\lambda(s)}\left[w_H^T\right]\tilde{\theta}_H\right) \\ -\gamma_G C_m e_1 G_m \begin{pmatrix} C_p e_{11} \\ e_{12} + \frac{a(s)}{\lambda(s)}\left[\tilde{\theta}_H^T w_H\right] \\ e_{13} \\ \gamma'\left(\left(\frac{a(s)}{\lambda(s)}\left[w_H^T\right]\right)^T \tilde{\theta}_1\right) \end{pmatrix} \end{bmatrix}
\end{aligned} \tag{4.29}$$

In order to proceed with analysis of the complete nonlinear system, the convolution operations in (4.29) must be realized in state-space form. Recall that $G_m(s)$ is a single-input single-output system and that

$$\int_0^t C_m e^{A_m(t-\tau)} B_m \begin{bmatrix} w_m \\ \gamma' \overline{w}_{HF} \end{bmatrix} d\tau$$

is actually the parallel action of $2n - 1 + n_H$ instances of this system. The state-space realization of this operation is

$$\dot{\hat{\zeta}} = A_\zeta \hat{\zeta} + B_\zeta \begin{bmatrix} w_m \\ \gamma' \overline{w}_{HF} \end{bmatrix} \tag{4.30}$$

$$\hat{\xi} = C_\zeta \hat{\zeta}, \tag{4.31}$$

where

$$A_\zeta = \begin{bmatrix} A_m & 0 & \cdots & 0 \\ 0 & A_m & & 0 \\ \vdots & & \ddots & \vdots \\ 0 & 0 & \cdots & A_m \end{bmatrix}, B_\zeta = \begin{bmatrix} B_m & 0 & \cdots & 0 \\ 0 & B_m & & 0 \\ \vdots & & \ddots & \vdots \\ 0 & 0 & \cdots & B_m \end{bmatrix},$$

$$C_\zeta = \begin{bmatrix} C_m & 0 & \cdots & 0 \\ 0 & C_m & & 0 \\ \vdots & & \ddots & \vdots \\ 0 & 0 & \cdots & C_m \end{bmatrix}.$$

Assume the steady-state solution of (4.30), denoted $\zeta(t)$, exists and has state-space representation

$$\begin{aligned} \dot{\zeta} &= A_\zeta \zeta + B_\zeta \begin{bmatrix} w_m \\ \gamma \overline{w}_{HF} \end{bmatrix} \\ \xi &= C_\zeta \zeta, \end{aligned}$$

and let $\tilde{\zeta} = \hat{\zeta} - \zeta$. Now to illustrate the idea, the first term in (4.29) is derived in the augmented state-space:

$$\begin{bmatrix} \dot{e}_1 \\ \dot{\tilde{\theta}} \end{bmatrix} = \begin{bmatrix} A_m & \frac{B_m}{\theta_3} \begin{bmatrix} w_m^T & \overline{w}_{HF}^T \end{bmatrix} \\ -\gamma_G \int_0^t C_m e^{A_m(t-\tau)} B_m \begin{bmatrix} w_m \\ \gamma \overline{w}_{HF} \end{bmatrix} d\tau C_m & 0 \end{bmatrix} \begin{bmatrix} e_1 \\ \tilde{\theta} \end{bmatrix}$$

$$\Rightarrow \begin{bmatrix} \dot{e}_1 \\ \dot{\tilde{\theta}} \\ \dot{\tilde{\zeta}} \end{bmatrix} = \begin{bmatrix} A_m & \frac{B_m}{\theta_3} \begin{bmatrix} w_m^T & \overline{w}_{HF}^T \end{bmatrix} & 0 \\ -\gamma_G C_\zeta \zeta C_m & 0 & 0 \\ 0 & 0 & A_\zeta \end{bmatrix} \begin{bmatrix} e_1 \\ \tilde{\theta} \\ \tilde{\zeta} \end{bmatrix} + \begin{bmatrix} 0 \\ -\gamma_G C_\zeta \tilde{\zeta} C_m e_1 \\ 0 \end{bmatrix}.$$

Continuing in this manner on the second and third terms in (4.29), grouping similar resulting terms, and augmenting another new state for $\frac{a(s)}{\lambda(s)}$ will lead to the complete expression

$$\dot{x} = A(t)x + f(t,x) + g(t,x_t) \tag{4.32}$$

where x is the new augmented state and x_t denotes a function of its history. Once favorable properties of (4.32) are established, the stability analysis can proceed using a variation of typical Lyapunov techniques. See for instance [15]. Establishing the asymptotic stability of (4.32) also validates using (4.27) as a local approximation of the nonlinear system. Until this point it is accepted that substituting $\overline{w}_H$ for w_H in (3.14) and (3.17), then linearizing the standard way, via partial derivatives, results in a legitimate estimate. The first term in (4.32) is merely an asymptotically stable, linear time-varying (LTV) matrix.

Now the stability of a system of the form (4.32) described by an FDE with desirable properties is shown. Define the Banach space Φ consisting of the set of continuous functions $\phi : \mathbb{R}^+ \rightarrow \mathbb{R}^{n_\phi}$, equipped with

$$\|\phi\| = \sup_{t \geq 0} \|\phi(t)\|.$$

Consider the asymptotically stable, LTV system

$$\dot{x} = A(t)x, \quad x \in \mathbb{R}^{n_x} \tag{4.33}$$

with $A(t)$ continuous in t and bounded. From [13] Theorem 4.12, for a continuous matrix $Q(t)$ satisfying

$$0 < c_1 I < Q(t) < c_2 I, \; \forall t > 0, \; Q(t) = Q^T(t)$$

there exists a continuously differentiable matrix $P(t)$ satisfying

$$0 < c_3 I < P(t) < c_4 I, \ \forall t > 0, \ P(t) = P^T(t),$$
$$-\dot{P}(t) = P(t)A(t) + A^T(t)P(t) + Q(t).$$

Equation (4.32) is a perturbed version of (4.33). Let

$$f : \mathbb{R}^+ \times \mathbb{R}^{n_x} \to \mathbb{R}^{n_x} \qquad \|f(t,x)\| \leq \kappa \|x\|^2,$$
$$g : \mathbb{R}^+ \times G \to \Phi \qquad \|g(t,x_t)\| \leq \rho \|x_t\| \|x\| \qquad G \subset \Phi.$$

Now, for the perturbed system (4.32), choose the Lyapunov function candidate $V(t,x) = x^T P(t)x$. The derivative of V along (4.32) is

$$\begin{aligned}
\dot{V}(t,x) &= x^T P(t)\left(f(t,x) + g(t,x_t)\right) + \left(f(t,x) + g(t,x_t)\right)^T P(t)x \\
&+ x^T \left(P(t)A(t) + A^T(t)P(t) + \dot{P}(t)\right) x \\
&= -x^T Q(t)x + 2\left(f(t,x) + g(t,x_t)\right)^T P(t)x \\
\Rightarrow \dot{V} &\leq -c_1 \|x\|^2 + 2c_4 \kappa \|x\|^3 + 2c_4 \rho \|x_t\| \|x\|^2 + 2c_4 \alpha \|x\|^2 \\
&= -\left(c_1 - 2c_4 \kappa \|x\| - 2c_4 \rho \|x_t\|\right) \|x\|^2. \qquad (4.34)
\end{aligned}$$

Define the neighborhood $\Phi_X = \{x_t \in \Phi : \|x_t\| < \min\{c_1/8c_4\kappa, c_1/8c_4\rho\}\}$. For $x_t \in \Phi_X$

$$\begin{aligned}
\dot{V} &\leq -\left(c_1 - 2c_4 \kappa \|x\| - 2c_4 \rho \|x_t\|\right) \|x\|^2 \\
&< -\frac{c_1}{2}\|x\|^2 \leq -\frac{c_1}{2c_4} V \\
\Rightarrow \dot{V} &< -\frac{c_1}{2c_4} V, \qquad (4.35)
\end{aligned}$$

where $c_1/2c_4 > 0$. The comparison system

$$\dot{y} = -\frac{c_1}{2c_4} y \triangleq h(y) \tag{4.36}$$

is introduced. This system is clearly exponentially stable, as it is merely a linear time-invariant (LTI) system with lone eigenvalue $\lambda_y = -c_1/2c_4 > 0$. Comparing (4.35) and (4.36) gives

$$\dot{V} < h(V). \tag{4.37}$$

Theorem 6.6.1 from [15] states that when (4.37) is true, that the exponential stability of (4.36) implies the exponential stability of the original system (4.32).

The above conclusion pertains to (4.32). The last step to verify (4.28) is locally exponentially stable is to show, when all convolution integrals are eliminated by state vector augmentation, that (4.28) indeed takes the form (4.32), with the same boundedness and continuity properties. Continuity properties of the Preisach operator and its right inverse are discussed in [16]. These results will be useful in showing the continuity of $\tilde{w}_{HF}$ as in (4.29). The second part of (**A5**) ensures a sufficient condition on the Preisach density function therein. Continuity and boundedness properties of many of the signals will follow from boundedness and continuity of the driving signal, along with the stability of $G_m(s)$ and $\frac{a(s)}{\lambda(s)}$.

Remark 4.1 *Note that in the context of Section 4.3,* $\|x\| \to 0$ *does not imply* $\|x_t\| \to 0$. *In fact, if at any single point in time* $\|x\| \neq 0$, *then* $\|x_t\|$ *will always be nonzero, regardless of what happens to* $\|x\|$ *thereafter.*

Remark 4.2 *Assumption (***A8***) considers* $d_H(t)$ *in (2.11) to be identically zero. Relaxing this assumption should not complicate the analysis. Since* $d_H(t)$ *will always be bounded, the output error should be ultimately bounded, with ultimate bound proportional to an upper bound on* $d_H(t)$.

Remark 4.3 *For sums of bounded, periodic signals, assumptions* (**B1**)-(**B2**) *will always be satisfied [13]. Periodic driving signals are common in many applications, e.g. [17], so often these are not stringent conditions.*

5. Simulation Results

Simulation results can now be introduced in order to better understand the behavior of the closed-loop system and to motivate further work. Several different aspects of interest will be explored. The simulations are performed on the complete closed-loop system, using software provided by Dr. Xiaobo Tan to simulate the Preisach operator and its approximate inverse. The algorithm for the inversion of the Preisach operator in [3] is an iterative algorithm, so it must be implemented in discrete time. Therefore, all simulations in this thesis are implemented in discrete-time, and parameter updates are performed according to the first-order approximation of (3.16):

$$\hat{\theta}(k+1) = \hat{\theta}(k) - \gamma_G e(k) G_d(k),$$

where $e(k)$ and $G_d(k)$ are the sampled data versions of $C_m e_1$ and

$$G_m\left(\begin{bmatrix} C_p x_p \\ w_{11} \\ w_2 \\ \gamma'\left(\left(\frac{a(s)}{\lambda(s)}[w_H^T]\right)^T \hat{\theta}_1 - w_H\right) \end{bmatrix}\right), \tag{5.1}$$

respectively.

In Section 5.1 the persistence of excitation of driving signals is examined. A vector $v(\cdot) : \mathbb{R}_+ \to \mathbb{R}^n$ is said to be persistently exciting (PE) of order n if there exist $\alpha_1, \alpha_2, \delta > 0$ such that

$$\alpha_2 I \geq \int_{t_0}^{t_0+\delta} v(\tau) v^T(\tau) d\tau \geq \alpha_1 I \tag{5.2}$$

for all $t_0 \geq 0$, where I is the $n \times n$ identity matrix [8]. Roughly speaking, a signal that is PE of order n can drive n adapted parameters to their true values in an MRAC system. The relationship between the initial conditions of the plant and hysteresis parameters is the

topic of Section 5.2. Let $\varphi(t,x_0)$ be a solution to

$$\dot{x} = f(x),$$

with an asymptotically stable equilibrium point $x = 0$. Then, the region of attraction is defined as the set of all points x_0 such that $\varphi(t,x_0)$ is defined for all $t \geq 0$ and

$$\lim_{t\to\infty} \varphi(t,x_0) = 0$$

in [13]. The main point of Section 5.2 is to illustrate how the initial estimate of the plant parameters affects the possible initial estimates of the hysteresis parameters, and vice versa. In addition, the region of attraction of zero output error and zero parameter error is investigated for the case when the hysteresis and plant parameter adaptation time-scales are sufficiently separated and when they are very near each other.

5.1 *Parameter Convergence*

Persistence of excitation of driving signals is well understood for open-loop identification problems. For linear systems with n parameters to be identified, the driving signal must have n unique nonzero spectral components (provided $Z_p(s)$ and $P_p(s)$ are coprime) [18]. PE conditions for linear MRAC systems depend instead on the internal regressor vectors, which cannot be explicitly chosen. A rule of thumb is to require the driving signal to have as many nonzero spectral components as the number of parameters to be estimated (the sum of the lengths of all regressors) [12]. Ioannou and Sun give sufficient conditions to guarantee parameter convergence when this type of driving signal is applied. In addition to assumptions **(A1)**-**(A4)**, $G_m(s)$ must also be strictly positive real for a classical MRAC with relative degree $n^* = 1$. For an increasingly complex linear system (larger number of parameters to be identified), the PE condition will require an increasing number of components in the driving signal.

Simulation Parameters	
Linear Dynamics	$G(s) = \frac{1121s+91650}{s^2+1475s+91650}$
Discrete Approximation	$G(z) = \frac{2.242z-1.8754}{z^2+.95z-1.5834}$
Driving Signal	$y_{\text{ref}} = 22\sin(2\pi 25t) + 22\sin(2\pi 50t)$
Sampling Period	$T = 2 \times 10^{-3}$
Adaptation Gains	$\gamma_G = 5 \times 10^{-5}$, $\gamma_H = 1 \times 10^{-2}$

Table 5.1: Parameter convergence simulation settings.

In [7] Tan and Baras introduce PE conditions in the identification of hysteresis parameters. Instead of depending on the number of spectral components, the hysteresis input signal ($v(t)$ in Fig. 2.4) must contain a sufficient number of reversals at specific levels. In other words, each discretization level should contain a local extremum of the signal $v(t)$.

PE conditions for the proposed closed-loop controller are not yet completely understood. Refer to the simulation parameters in Table 5.1. The amplitude of the driving signal is chosen in order to drive the hysteresis operator very near its upper and lower saturation levels. This is to ensure that each level in the truncated Preisach plane is reached. For each simulation in this Section 5.1, the parameter errors will be calculated as

$$\begin{aligned} e_G(t) &= 100 \sum_{i=1}^{2n-1} \left(\left| \frac{\hat{\theta}_{Gi}(t) - \theta_{Gi}}{\theta_{Gi}} \right| \right) \text{ and} \\ e_H(t) &= 100 \sum_{i=1}^{n_H} \left(\left| \frac{\hat{\theta}_{Hi}(t) - \theta_{Hi}}{\theta_{Hi}} \right| \right). \end{aligned}$$

The first simulation case has discretization level $L = 4$ and initial parameter estimate $\hat{\theta} = 1.05\theta$. The matrices Ω_f and Ω_s are calculated numerically with sampling period $T = 2 \times 10^{-8}$, which gives a million samples for every period of the driving signal. For $L = 4$, both of these matrices have full rank, i.e. $\text{rank}[\Omega_f] = 3$ and $\text{rank}[\Omega_s] = 11$. Fig. 5.1 shows

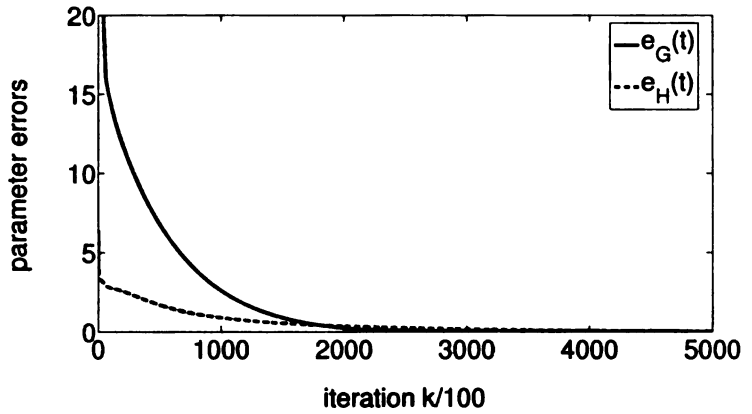

Figure 5.1: Parameter error for case $L = 4$.

that when the plant and hysteresis parameters are updated using the adaptation gains in Table 5.1, the signal drives all parameter estimates to their true values. Thus, for this case the above approach produces a persistently exciting driving signal.

The implication of the previous example is significant. In this particular case, there are only two frequency components in the driving signal and all 14 parameter estimates reach their true values. For $L = 8$, on the other hand, Ω_s is not positive definite, in particular, $\text{rank}[\Omega_s] = 30$ while $n_H = 37$. From Fig. 5.2, it is clear that the parameter estimates do not converge to their true values, but rather some other steady-state. It is encouraging to note, however, that while the parameter estimates do not converge, the output error, computed as

$$e_L(t) = \log|y(t) - y_m(t)|$$

continues to approach zero as time approaches infinity, as in Fig. 5.3. The downward spike is when the error $y(t) - y_m(t)$ switches signs. This means that under appropriate conditions it may be possible to guarantee perfect tracking in the absence of a PE driving signal, which makes the proposed controller much more practical.

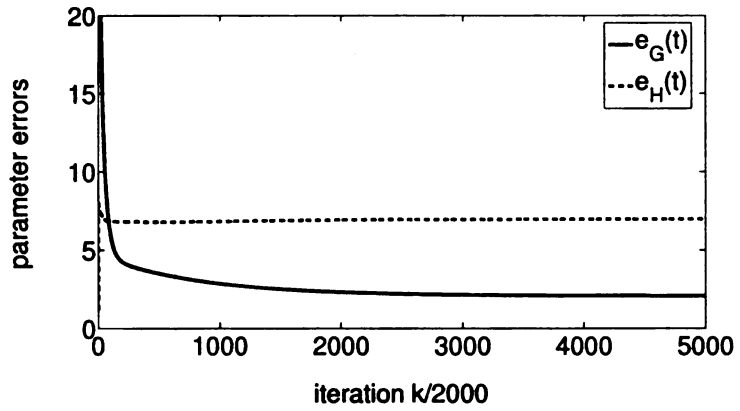

Figure 5.2: Parameter error for case $L = 8$.

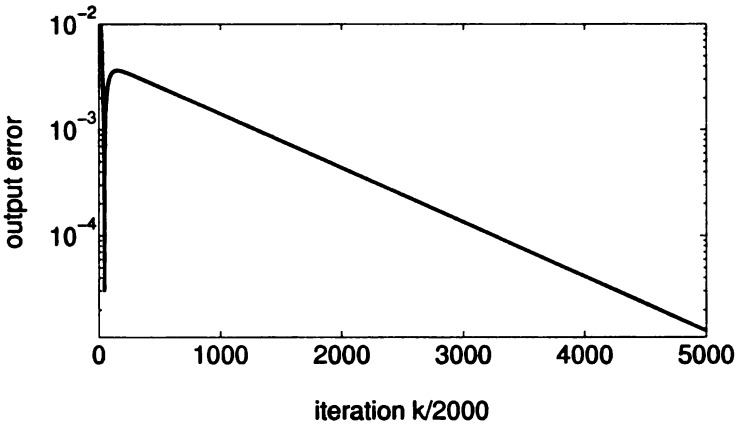

Figure 5.3: Output error for case $L = 8$.

5.2 *Region of Attraction*

In this section, the effects that the separation of time-scales and initial parameter estimates have on convergence are investigated. Since it is impossible to completely classify the region of attraction of the $2n - 1 + n_H$-dimensional system, the problem is restricted to a two degree-of-freedom (DOF) problem instead. Consider two design parameters a and b. The initial parameter estimates are governed by these parameters as

$$\hat{\theta}_G(0) = a\theta_G \quad \text{and} \quad \hat{\theta}_H(0) = b\theta_H. \tag{5.3}$$

When $a = b = 1$ the initial parameter estimates are the true parameter values, and the output error is identically zero. Fig. 5.4 shows the region of attraction in the $a - b$ plane. Two cases are shown: the solid line is for $\gamma_H = 10^{-2}$ and the dashed line is for $\gamma_H = 10^{-1}$. In the first case, the hysteresis parameters evolve at a rate that is approximately ten times slower than the plant parameters. This is considered a sufficient separation of time scales for this particular system, as decreasing γ_H further does not have a significant impact on the region of attraction. In the second case, the hysteresis parameters evolve at nearly the same rate as the plant parameters. It is clear from Fig. 5.4 that while there seems to be little regularity or symmetry to the encircled regions, the separation of time scales brings the added benefit of a larger region of attraction. In fact the (dimensionless) area of each encircled region can be easily computed:

$$\text{AREA}_{\text{solid}} = 3.9453 \quad \text{and} \quad \text{AREA}_{\text{dashed}} = 2.5122.$$

In this case, the separation of time scales increases the two DOF region of attraction over 57%. This snapshot of the respective regions of attraction are in no way the true maximal regions of attraction, which can only be represented as a $2n - 1 + n_H$-dimensional volume. However, even in this simplified case the benefit is clearly evident.

It is also worth noting that the region in the $a - b$ plane to the immediate right of the encircled regions still gives output error stability, but the parameters do not converge their true values. In the rest of the $a - b$ plane, outside of the encircled areas, the parameter estimates and the output error are unstable. As such, one cannot generalize that the complete nonlinear system will always be stable, without placing sufficiently small limits (e.g. via parameter projection) on the parameter estimates.

From Fig. 5.4 it is clear that in this simplified investigation of the region of attraction, that both an adequate separation of time scales and and a more precise initial estimate of the plant (hysteresis) parameters allows more variation of the initial estimate of the hysteresis

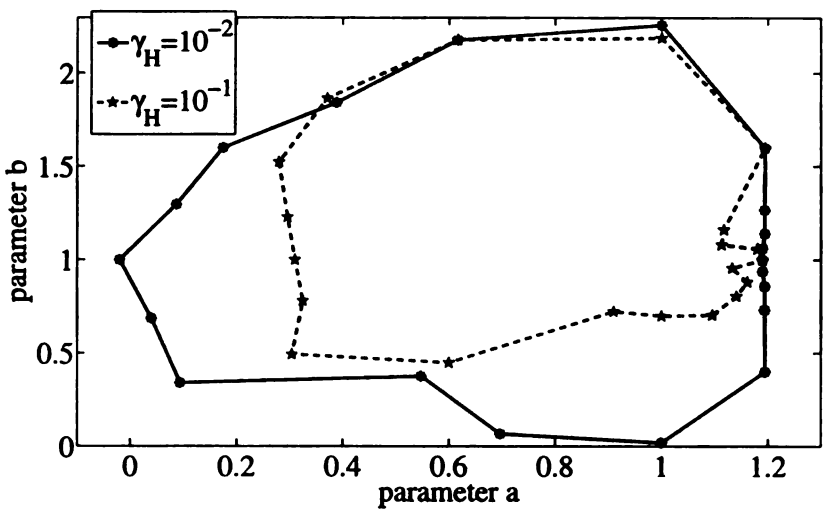

Figure 5.4: Comparison of regions of attraction.

(plant) parameters.

6. Future Work

There is still much work to be done regarding this particular control scheme. The analysis herein is based completely on "linearizing" the error and adaptation dynamics, then performing averaging. The local exponential stability via a Lyapunov argument is based on the linear system's stability being proven by averaging. In the identification problem in [6] and repeated in Section 4.1, averaging is applied to the complete nonlinear system. Linearization is only used to show the stability of the averaged nonlinear system. This allows the authors to estimate the region of attraction. In general, averaging the closed-loop nonlinear system in Section 4.2, rather than linearizing prior to averaging, may provide more useful insight into the system behavior. This will require a thorough understanding of the signal w_H, so that a new averaging theorem can be derived, or the work regarding nonlinear averaging by Teel, Moreau and Nešić in [19] or the work regarding averaging with hysteresis by Pokrovskii, Rasskazov and Vladimirov in [20] can be applied.

The PD requirement on Ω_f and Ω_s only guarantee parameter convergence in a neighborhood of the origin. Finding an analytical expression for the region of attraction will demonstrate how practical this control scheme will be in systems with poor initial parameter estimates. Additionally, one may investigate whether the region of attraction is in any way dependent on the magnitude of separation of time scales. In this thesis, the aforementioned PD conditions were satisfied in an ad hoc manner. A signal was chosen, and then the matrices were computed to show whether or not the signal would lead to convergence. It will be of interest to find sufficient conditions on the driving signal that will lead to both matrices being PD. In Section 5.1, simulations showed that when conditions (4.18) and (4.19) are not satisfied, the output error may still converge to zero. This needs rigorous analysis to establish under which conditions output error convergence can be guaranteed.

References

[1] X. Tan, "Control of smart actuators," Ph.D. dissertation, University of Maryland, College Park, 2002, available at http://www.egr.msu.edu/~xbtan/papers.html.

[2] X. Tan and J. S. Baras, "Modeling and control of a magnetostrictive actuator," in *Proceedings of IEEE Conference on Decision and Control*, 2002, pp. 866–872.

[3] ——, "Modeling and control of hysteresis in magnetostrictive actuators," *Automatica*, vol. 40, no. 9, pp. 1469–1480, 2004.

[4] G. Tao and P. V. Kokotovic, "Adaptive control of plants with unknown hysteresis," *IEEE Transactions on Automatic Control*, vol. 40, no. 2, pp. 200–212, 1995.

[5] ——, *Adaptive Control of Systems with Actuator and Sensor Nonlinearities*. New York: John Wiley & Sons, Inc., 1996.

[6] X. Tan and H. K. Khalil, "Control of unknown dynamic hysteretic systems using slow adaptation: Preliminary results," in *Proceedings of the 26th American Control Conference*, New York, NY, 2007, pp. 3294–3299.

[7] X. Tan and J. S. Baras, "Adaptive identification and control of hysteresis in smart materials," *IEEE Transactions on Automatic Control*, vol. 50, no. 6, pp. 827–839, 2005.

[8] S. Sastry and M. Bodson, *Adaptive Control*. Englewood Cliffs, NJ: Prentice Hall, 1989.

[9] P. Kokotović, H. K. Khalil, and J. O'Reilly, *Singular Perturbation Methods in Control: Analysis and Design*. Philadelphia: Society for Industrial and Applied Mathematics, 1999.

[10] I. D. Mayergoyz, *Mathematical Models of Hysteresis and Their Applications*. New York, NY: Elsevier, 2003.

[11] J. J. Reynolds, X. Tan, and H. K. Khalil, "Closed-loop analysis of slow adaptation in the control of unknown dynamic hysteretic systems," in *Proceedings of the 46th IEEE Conference on Decision and Control*, New Orleans, LA, 2007, to appear.

[12] P. A. Ioannou and J. Sun, *Robust Adaptive Control*. Prentice-Hall, 1995.

[13] H. K. Khalil, *Nonlinear Systems*, 3rd ed. Upper Saddle River, New Jersey: Prentice Hall, 2002.

[14] D. S. Bernstein, *Matrix Mathematics: Theory, Facts and Formulas with Application to Linear Systems Theory*. Princeton, New Jersey: Princeton University Press, 2005.

[15] A. N. Michel and K. Wang, *Qualitative Theory of Dynamical Systems*. New York, NY: Marcel Dekker, Inc., 1995.

[16] R. V. Iyer, X. Tan, and P. S. Krishnaprasad, "Approximate inversion of the Preisach hysteresis operator with application to control of smart actuators," *IEEE Transactions on Automatic Control*, vol. 50, no. 6, pp. 798–810, 2005.

[17] D. Croft, G. Shed, and S. Devasia, "Creep, hysteresis, and vibration compensation for piezoactuators: Atomic force microscopy application," *Journal of Dynamic Systems, Measurement, and Control*, vol. 123, no. 1, pp. 35–43, 2001.

[18] B. D. O. Anderson, R. R. Bitmead, C. R. Johnson, Jr., P. V. Kokotovic, R. L. Kosut, I. M. Y. Mareels, L. Praly, and B. D. Riedle, *Stability of Adaptive Systems: Passivity and Averaging Analysis*. Cambridge, MA: The MIT Press, 1986.

[19] A. R. Teel, L. Moreau, and D. Nešić, "A unified framework for input-to-state stability in systems with two time scales," *IEEE Transactions on Automatic Control*, vol. 48, no. 9, pp. 1526–1544, Sept. 2003.

[20] A. Pokrovskii, O. Rasskazov, and A. Vladimirov, "Averaging principle for differential equations with hysteresis," University College Cork, Ireland, Tech. Rep., 2004.